Radio Science, Volume 33, Number 6, Pages 1617–1639, November–December 1998

Constraints on the polarization purity of a Stokes microwave radiometer

Christopher S. Ruf

Department of Electrical Engineering, Pennsylvania State University, University Park

Abstract. Measurement of the third and fourth Stokes parameters of microwave thermal emission can be degraded by nonideal radiometer characteristics. Of particular importance is the level of polarization purity and the knowledge of polarization impurity on the part of the instrument. An explicit relationship is developed between the true Stokes parameters and the measurements, as functions of nonideal polarization characteristics. In principle, knowledge of the characteristics allows the degradation to be removed by a postprocessing calibration procedure. However, errors in the knowledge are possible, resulting from inexact initial testing and/or subsequent drifting of the instrument. The effects of these errors on overall calibration are considered. It is found that there is considerably greater tolerance to the errors when incoherent detection is used (differencing $\pm 45°$ linear and left- or right-hand circular polarizations), as opposed to coherent detection (direct cross correlation of vertical and horizontal linear polarizations). This is particularly true when cross-polar leakage is imbalanced. The level of nominal polarization purity that is required is also more relaxed in the incoherent case. On the other hand, coherent detection has the capability for superior performance with regard to precision.

1. Introduction

Estimation of ocean surface wind speed by microwave radiometers using linearly polarized brightness temperatures is a well-established technique [e.g., *Wilheit and Chang*, 1980; *Goodberlet et al*., 1989]. Early investigations into the anisotropy of microwave emission by the ocean surface identified wind direction as the cause [*Bespalova et al*., 1982; *Etkin et al*., 1991; *Wentz*, 1992]. The results suggest that a properly calibrated spaceborne microwave radiometer should be sensitive to both wind speed and direction. Subsequently, numerous investigations have considered the additional information about wind direction contained in the third and fourth Stokes parameters of the emission (defined below) [e.g., *Yueh et al*., 1995; *Gasiewski and Piepmeier*, 1996; *Skou and Laursen*, 1996]. Each of these studies involved the fabrication of a polarimetric radiometer capable of measuring additional Stokes parameters beyond the conventional vertical and horizontal linear polarizations (V- and H-pol). In this paper we consider some constraints on the design and calibration of such a radiometer imposed by absolute accuracy and precision requirements. Of particular interest are the levels of polarization purity and knowledge of polarization impurity on the part of the antenna subsystem that are needed to adequately estimate wind direction.

There are two popular approaches to the design of a polarimetric radiometer, using either coherent or incoherent detection, and they are both considered here. The two approaches are defined in section 2. Section 2 also briefly addresses the relationship between wind direction and brightness temperature, but only in detail sufficient to provide a general guideline for the accuracy and precision requirements of the measurements. Section 3 identifies the effects that nonideal antenna polarization characteristics have on measurement of the Stokes parameters. A relationship between the true Stokes parameters and the actual measurements is developed, which must be inverted as part of a complete calibration algorithm. Section 4 examines the calibration inaccuracies that result when the inversion is performed with inexact knowledge of the polarization characteristics. Section 5 addresses the propagation of noise through the inversion procedure and the relationship between measurement noise, ΔT, and the precision of wind direction estimates. Section 6 concludes with a discussion of the implications that these results have on

Paper number 98RS02773.
0048-6604/98/98RS-02773$11.00

the design and testing of a polarimetric radiometer antenna subsystem.

2. Stokes Parameters and Ocean Wind Direction

A polarimetric microwave radiometer measures V- and H-pol brightness temperatures in the conventional manner. If $\mathbf{E} = E_V\hat{V} + E_H\hat{H}$ is the electric field incident on the radiometer's antenna, then T_V and T_H are given by

$$T_V = c\langle|E_V|^2\rangle \tag{1}$$

$$T_H = c\langle|E_H|^2\rangle \tag{2}$$

where $\hat{V}$ and $\hat{H}$ are vertical and horizontal unit vectors, and $c = \lambda^2/k\eta B$, where λ is the RF center frequency, k is the Boltzmann constant, η is the intrinsic impedance of free space, and B is the RF bandwidth. Measurement of the third and fourth Stokes parameters can be carried out by either coherent or incoherent means [e.g., *Ishimaru*, 1991]. Coherent detection implies that a direct cross correlation is performed of the vertical and horizontal components of the incident electric field, as described by

$$T_3 + jT_4 = 2c\langle|E_V E_H^*|\rangle \tag{3}$$

Here the third and fourth Stokes parameters are designated T_3 and T_4, rather than the conventional U and V, to avoid confusion with the vertical coordinate V. The asterisk denotes the complex conjugate. The coherent approach has been used in several polarimetric radiometer designs [*Gasiewski and Piepmeier*, 1996; *Skou and Laursen*, 1996]. Coherent detection has several attractive features. If the complex correlation is performed digitally, then that portion of the instrument will have linearity, gain, and amplitude and phase imbalances which are highly repeatable over time. Also, only one complex-correlation channel is required, as opposed to the four-channel system required in the incoherent case.

Incoherent detection relies on the following relationships between the Stokes parameters and other, readily measured, brightness temperatures:

$$T_P = (T_V + T_H)/2 + c\ \mathrm{Re}\ \{\langle|E_V E_H^*|\rangle\} \tag{4}$$

$$T_M = (T_V + T_H)/2 - c\ \mathrm{Re}\ \{\langle|E_V E_H^*|\rangle\} \tag{5}$$

$$T_L = (T_V + T_H)/2 + c\ \mathrm{Im}\ \{\langle|E_V E_H^*|\rangle\} \tag{6}$$

$$T_R = (T_V + T_H)/2 - c\ \mathrm{Im}\ \{\langle|E_V E_H^*|\rangle\} \tag{7}$$

where T_P (T_M) is +45° (−45°) linear polarization and T_L (T_R) is left-hand (right-hand) circular polarization (LHCP and RHCP). These additional polarization channels can be formed from the standard V- and H-pol outputs of an antenna using 0° and 180° hybrids for T_P and T_M and ±90° quadrature hybrids for T_L and T_R [*Yueh et al*., 1995]. The incoherent estimates of T_3 and T_4 follow as

$$T_{3_{inc}} = T_P - T_M \tag{8}$$

$$T_{4_{inc}} = T_L - T_R \tag{9}$$

The incoherent approach has also been used by several polarimetric radiometers [*Yueh et al*., 1995; *Sollner and Suss*, 1996]. Its principle advantage is the use of existing, well-understood incoherent detection circuitry following the polarization forming hybrids. We show below that there may also be significant advantages to the incoherent approach with regard to the stability of its absolute calibration.

Numerous investigations have considered the relationship between the Stokes parameters and microwave emission from the wind-roughened ocean, with particular emphasis on the relative azimuth directions of the wind and the radiometer look angle [e.g., *Wentz*, 1992; *Yueh et al*., 1994a, b]. For the sensitivity analyses presented here, we consider a typical instrument configuration consisting of a polarimetric radiometer operating at 19.35 GHz with a 50° incidence angle. We employ model functions that relate the Stokes parameters to the wind speed and direction that are extracted from empirical data presented in the literature from aircraft overflights of buoys. A nominal 12 m/s wind speed is assumed in determining T_V, T_H, and T_3. A 10 m/s wind speed is assumed for T_4. The slight discrepancy in wind speed results from extracting model functions for T_V, T_H, and T_3 from *Yueh et al*. [1995] and for T_4 from *Wilson and Yueh* [1996]. The resulting model functions for the brightness temperatures are

$$T_V = 172 + 1.5\cos\theta + 0.95\cos 2\theta \tag{10a}$$

$$T_H = 113 + 0.5\cos\theta - 1.0\cos 2\theta \tag{10b}$$

$$T_3 = -1.25\sin\theta - 1.7\sin 2\theta \tag{10c}$$

$$T_4 = 0.5\sin 2\theta \tag{10d}$$

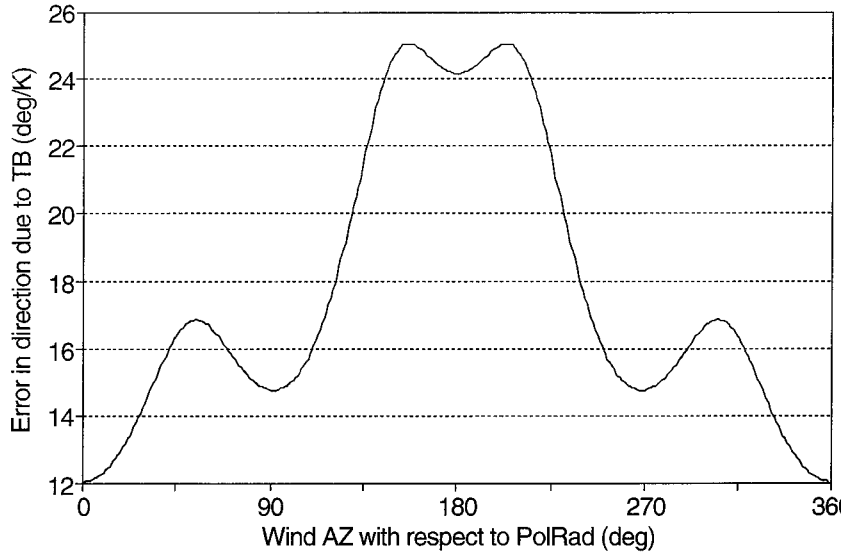

Figure 1. Sensitivity of estimated wind direction to errors in the four Stokes parameters, as a function of the relative angle between the wind direction and the azimuth angle of the radiometer observation (assuming 19.35-GHz observations at a 50° angle of incidence with 10–12 m/s winds). Upwind (0°) observations are most tolerant of measurement errors, while 157° and 203° observations are most sensitive. A measurement error of 0.4 K corresponds to an error in wind direction of 5°–10°.

where θ is the wind direction relative to the azimuth look angle of the radiometer. This model results from direct curve fits of aircraft brightness temperatures to surface buoy data and so also includes second-order atmospheric effects. However, for purposes of our analysis the relations in (10) need not be exact. The approximate magnitudes of the Stokes parameters, and their relative sensitivities to wind direction, are of primary interest here.

Equations (10) can be used to establish a sensitivity relationship between small errors in the measurements and in the inferred wind direction. For small errors the change in θ corresponding to a change in T_V is given by

$$\delta\theta|_{T_V} = \delta T\left(\frac{dT_V}{d\theta}\right)^{-1} \tag{11}$$

where δT is the change in T_V and where the derivative follows from (10a). Similar expressions result for small changes in each of the measurements. Assume that an inversion algorithm exists that estimates wind direction from the measurements. We are interested here in the incremental effects on that algorithm of small errors in the measurements, such as might be caused by uncorrected instrument drifts and additive noise. If the drifts and/or noise are uncorrelated, their net effect on the estimate of wind direction will be reduced by averaging. The total incremental change in θ follows as

$$\delta\theta = [(\delta\theta|_{T_V})^{-2} + (\delta\theta|_{T_H})^{-2} + (\delta\theta|_{T_3})^{-2} + (\delta\theta|_{T_4})^{-2}]^{-1/2} \tag{12}$$

where we have assumed Gaussian statistics and summed the inverse variances of each contribution. Assuming that the incremental change δT in each measurement is similar, it can be factored out of the summation in (12) and used to normalize $\delta\theta$. The result is a sensitivity scale factor $\delta\theta/\delta T$, which translates errors in brightness temperature to errors in the estimation of wind direction. A plot of this scale factor versus wind direction is shown in Figure 1. Note that maximum sensitivity to measurement error occurs near downwind ($\theta \approx 157°$ and 203°) and minimum sensitivity occurs upwind ($\theta = 0°$). Measurement errors in the 0.3- to 0.5-K range correspond to errors in wind direction in the range 4°–12°, depending on wind direction. This level of error is roughly consistent with the retrieval accuracy of one polarimetric radiometer wind direction algorithm [*Gaiser et al.*, 1996]. On the basis of these results we will use as a general guideline the requirement that

each of the four Stokes parameters be corrected for polarization impurity with 0.4-K accuracy. It should be noted that numerous other sources of error in the retrieval of wind direction, for example, from receiver gain imbalances and nonlinearities, will add to the 5°–10° error. If these other sources become sufficiently large, then the 0.4-K requirement on polarization accuracy would need to be tightened accordingly.

3. Model for Nonideal Antenna Measurement of Stokes Parameters

In practice, there are a number of unavoidable, nonideal characteristics of the antenna subsystem that result in contaminated measurements of the true Stokes parameters. For example, (1) typical offset reflector antenna designs can introduce significant cross polarization; (2) the orthomode transducer often used on antenna feed horns to separate orthogonal linearly polarized components of the incident field has leakage signals from the unwanted polarization; and (3) the hybrids used to form ±45° linear polarization and LHCP/RHCP will have small-amplitude imbalances and phase deviations from ideal 0°, 180°, and ±90°. All of these characteristics can be modeled by incorporating the nonideal hardware behavior into the relationship between the incident electric field and the radiometer's detected output. This relationship is developed in detail in the appendix. The results are summarized here. Denote nonideal measured values for the Stokes parameters by T'_V, T'_H, T'_3, and T'_4, and denote true values for the parameters by T_V, T_H, T_3, and T_4. They are related by

$$T'_V = [T_V + i_V T_H + \sqrt{i_V}(T_3 \cos \phi_V + T_4 \sin \phi_V)]/(1 + i_V) \tag{13}$$

$$T'_H = [T_H + i_H T_V + \sqrt{i_H}(T_3 \cos \phi_H - T_4 \sin \phi_H)]/(1 + i_H) \tag{14}$$

$$\begin{aligned} T'_{3_{coh}} = {} & \{T_3[1 + \sqrt{i_V i_H} \cos (\phi_V - \phi_H)] \\ & + T_4 \sqrt{i_V i_H} \sin (\phi_V - \phi_H) + 2T_V \sqrt{i_H} \cos \phi_H \\ & + 2T_H \sqrt{i_V} \cos \phi_V\}/\sqrt{(1 + i_V)(1 + i_H)} \end{aligned} \tag{15}$$

$$\begin{aligned} T'_{4_{coh}} = {} & \{T_4[1 - \sqrt{i_V i_H} \cos (\phi_V - \phi_H)] \\ & + T_3 \sqrt{i_V i_H} \sin (\phi_V - \phi_H) - 2T_V \sqrt{i_H} \sin \phi_H \\ & + 2T_H \sqrt{i_V} \sin \phi_V\}/\sqrt{(1 + i_V)(1 + i_H)} \end{aligned} \tag{16}$$

$$\begin{aligned} T'_{3_{inc}} = {} & T_3[(1 - i_P)/(1 + i_P) + (1 - i_M)/(1 + i_M)]/2 \\ & - T_4[\sqrt{i_P} \sin \phi_P/(1 + i_P) + \sqrt{i_M} \sin \phi_M/(1 + i_M)] \\ & + T_V[(1 + 2\sqrt{i_P} \cos \phi_P + i_P)/(1 + i_P) \\ & - (1 + 2\sqrt{i_M} \cos \phi_M + i_M)/(1 + i_M)]/2 \\ & + T_H[(1 - 2\sqrt{i_P} \cos \phi_P + i_P)/(1 + i_P) \\ & - (1 - 2\sqrt{i_M} \cos \phi_M + i_M)/(1 + i_M)]/2 \end{aligned} \tag{17}$$

$$\begin{aligned} T'_{4_{inc}} = {} & T_4\left(\frac{\sqrt{e_L} \cos \phi_L}{1 + e_L} + \frac{\sqrt{e_R} \cos \phi_R}{1 + e_R}\right) \\ & + T_3\left(\frac{\sqrt{e_L} \sin \phi_L}{1 + e_L} + \frac{\sqrt{e_R} \sin \phi_R}{1 + e_R}\right) \\ & + T_V\left(\frac{1}{1 + e_L} - \frac{1}{1 + e_R}\right) + T_H\left(\frac{e_L}{1 + e_L} - \frac{e_R}{1 + e_R}\right) \end{aligned} \tag{18}$$

where (1) i_V (i_H) is the isolation at the vertical (horizontal) port from leakage of the horizontal (vertical) signal; (2) ϕ_V (ϕ_H) is the phase of the horizontal (vertical) signal with respect to the vertical (horizontal) signal leaving the vertical (horizontal) port; (3) i_P (i_M) is the isolation at the +45° (−45°) port from leakage of the −45° (+45°) signal; (4) ϕ_P (ϕ_M) is the phase of the −45° (+45°) signal with respect to the +45° (−45°) signal leaving the +45° (−45°) port; (5) e_L (e_R) is the eccentricity of the LHCP (RHCP) channel, defined as the ratio of sensitivity to horizontal versus vertical polarized signals; and (5) ϕ_L (ϕ_R) is the phase deviation from −90° (+90°) of the quadrature hybrid. Under ideal conditions we have $i_V = i_H = i_P = i_M = 0$, $e_L = e_R = 1$, and $\phi_L = \phi_R = 0°$, which gives $T'_x = T_x$ for x = V, H, 3, and 4 (for both coherent and incoherent detection).

As an example, cross-polar leakage can result from rotation of the local orientation of the polarization axes (at the antenna) with respect to the Earth reference frame. If an antenna is rotated by an angle θ about an axis parallel to its main-beam boresight, then the local V, H, P, and M orientations will be rotated by the same amount. Using (13)–(18), this corresponds to isolation levels of $i_V = i_H = i_P = i_M = (\sin \theta/\cos \theta)^2$, relative phases in the leakage of $|\phi_V - \phi_H| = |\phi_P - \phi_M| = 180°$, and an eccentricity of $e_L = e_R = 1$. For example, rotation by 1° corresponds to an isolation of 0.0003 (35 dB). Equiv-

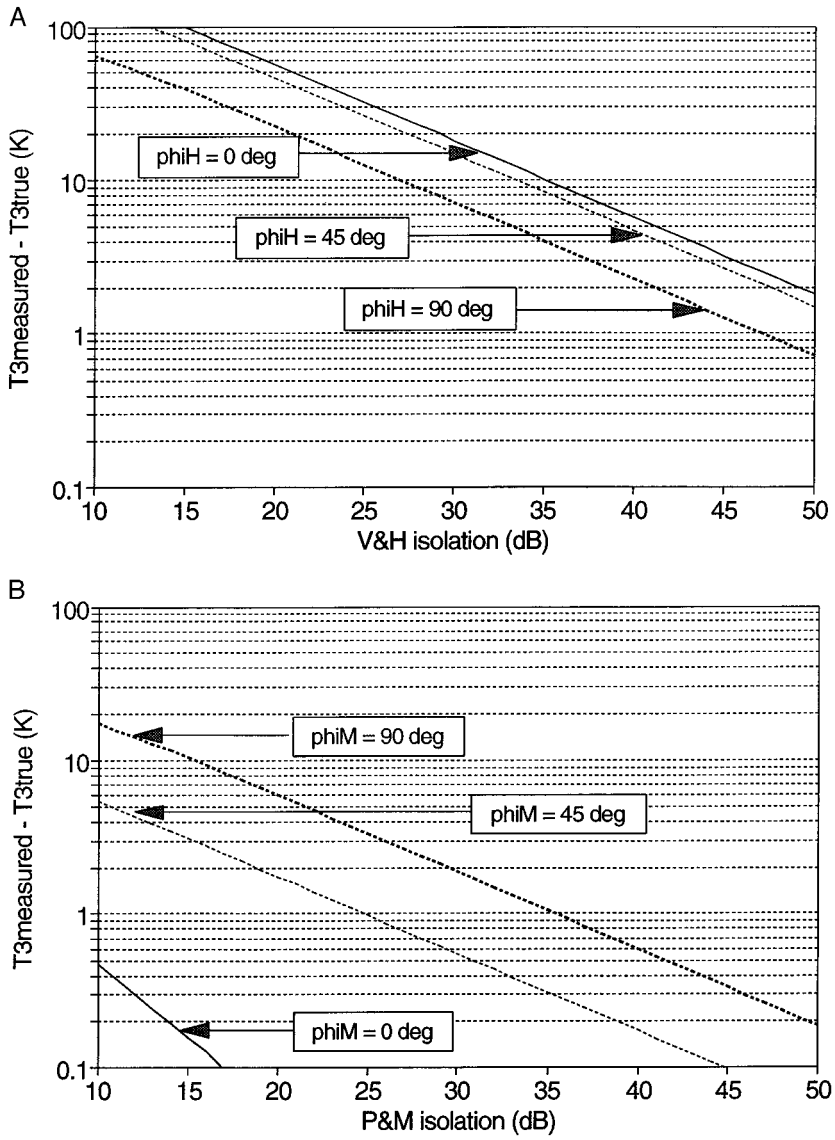

Figure 2. Contamination of the true third Stokes parameter T_3 by polarization impurities in the antenna subsystem. In the (a) coherent case, T_3 has been altered by several kelvins even with extremely high quality isolation between the vertical and horizontal polarization (V- and H-pol) channels (~40 dB). In the (b) incoherent case, moderate levels of isolation between the P- and M-pol channels (~20 dB) result in very little contamination, provided the leakage is in phase with the primary signal. In all cases, $\phi_V = \phi_P = 0°$.

alently, knowledge of the antenna orientation with 1° of accuracy corresponds to possible errors in knowledge of the isolation of −35 dB. (Here and in the following analysis we use positive decibel values to denote the level of isolation and negative values for the error in knowledge of the isolation.)

Examples of the error introduced by (15) and (17) into the measurement of T_3 are shown in Figure 2. In the coherent case, the error, $T'_{3_{coh}} - T_3$, is shown in Figure 2a versus the level of isolation between the vertical and horizontal ports and for various differences in phase, $\phi_V - \phi_H$, between the leakage. Even at the very high isolation level of 40 dB, T'_3 is still in error by 2–6 K, depending on $\phi_V - \phi_H$. This level of error is comparable to the value of T_3 itself and must be corrected to adequately calibrate the radiometer.

With incoherent detection, the error, $T'_{3_{inc}} - T_3$, shown in Figure 2b is generally at a much lower level. Reasons for this are discussed at length in the next section. Note that the error also depends strongly on the phase difference, $\phi_P - \phi_M$, between the leakage.

Equations (13)–(18) describe a linear transformation from the desired Stokes parameters to the actual measurements. Define the mappings $\mathbf{R}_{coh}$ and $\mathbf{R}_{inc}$ according to (13)–(18), so that

$$\mathbf{T}'_{coh} = \mathbf{R}_{coh}\mathbf{T} \tag{19}$$

$$\mathbf{T}'_{inc} = \mathbf{R}_{inc}\mathbf{T} \tag{20}$$

where $\mathbf{T} = (T_V, T_H, T_3, T_4)$, $\mathbf{T}' = (T'_V, T'_H, T'_3, T'_4)$, $T_{V_{coh}} = T_{V_{inc}}$, and $T_{H_{coh}} = T_{H_{inc}}$. In the next two sections, we consider the behavior of the inverse of (19) and (20) with respect to measurement accuracy and precision.

4. Accuracy of Stokes Measurements

The mappings (19)–(20) can be inverted exactly, provided there is no error in knowledge of the various isolation and eccentricity magnitudes and phases included in (13)–(18). In practice, however, the elements of $\mathbf{R}_{coh}$ and $\mathbf{R}_{inc}$ are subject to two sources of error. First, there are limitations to the accuracy with which the elements can be measured and/or modeled. In addition, the levels of isolation and the phases of the leakage may drift in between calibration tests. The sensitivity to these errors is assessed by computing the corrupted measurements, $\mathbf{T}'_{coh}$ and $\mathbf{T}'_{inc}$, using nominal values for $\mathbf{R}_{coh}$ and $\mathbf{R}_{inc}$ and then inverting them using slightly different values to retrieve $\mathbf{T}_{coh}$ and $\mathbf{T}_{inc}$. Discrepancies in the resulting Stokes parameters represent errors in the calibration. Details of this simulation follow.

Errors in knowledge of the hardware specifications are modeled by zero mean normally distributed random variables. The error analysis is performed as follows: Nominal values are assumed for the Stokes parameters over open ocean at 10–12 m/s wind speed, as described in the previous section, and at a relative azimuth angle of 45°. Values for each of the hardware specifications are also assumed. The hardware values are varied as part of a parametric analysis. Measurements of $\mathbf{T}'_{coh}$ and $\mathbf{T}'_{inc}$ are then computed using (19)–(20). The effects of error in knowledge of the hardware specifications are determined by a numerical simulation. Several thousand realizations of the inversion of (19)–(20) are generated, in which, prior to matrix inversion, elements of $\mathbf{R}$ are randomly perturbed by adding Gaussian "noise" to each of the hardware specifications. The noise represents errors in knowledge, and the standard deviations of the Gaussian perturbations are also varied as part of the parametric analysis. Finally, for each realization the estimated values of the Stokes parameters (after inversion) are recorded, and their standard deviations are computed. We note here that the mean value of the realizations was also computed, and no significant bias was noted, relative to the true Stokes parameters, for any of the parametric variables. A numerical simulation approach was used because the forward mapping $\mathbf{R}$ and especially the inverse mapping $\mathbf{R}^{-1}$ are nonlinear in the various hardware specifications, which makes an analytical solution less tractable.

4.1. Coherent Detection of T_3 and T_4

Parametric analysis of the coherent method of detection involves variations in the isolation between V- and H-pol channels, the phase of the leakage signals in each channel, and the standard deviations of each of these four values (representing the error in knowledge of the value). We consider first the effects on T_3 calibration of errors in knowledge of the level of isolation. In Figure 3a the level of isolation between channels is varied from 10 to 50 dB. Knowledge of the level of isolation is assumed to be accurate to either −40 or −50 dB (for example, isolation of 30 dB with −40-dB knowledge implies that the leakage is 30 dB below the primary signal and that its level is known to one part in ten). Three cases of relative phase between the leakage signals are also considered. (We note here that for a given relative phase, the absolute phase of the leakage had no significant effect on the behavior of the error. Results are shown only for relative phases of 0°, 45°, and 90°. The behavior at 180° was similar to that at 0°, that at 135°, 225°, and 315° was similar to 45°, and that at 270° was similar to 90°.) Figure 3a shows the rms error in T_3, σ_{T_3} that results from attempting to correct for the polarization impurity with inaccurate knowledge of the level of leakage. In Figure 3a, σ_{T_3} is lowest when the relative knowledge of the level of leakage is best. This occurs when either the leakage is large or the absolute knowledge is small. Note that when the level of isolation becomes comparable to the knowledge, the behavior of σ_{T_3} tends to level out. This can be explained by noting, for example, that if the isolation is known to −40 dB, then it makes little difference whether the isolation itself is 40 or 50 dB. Finally,

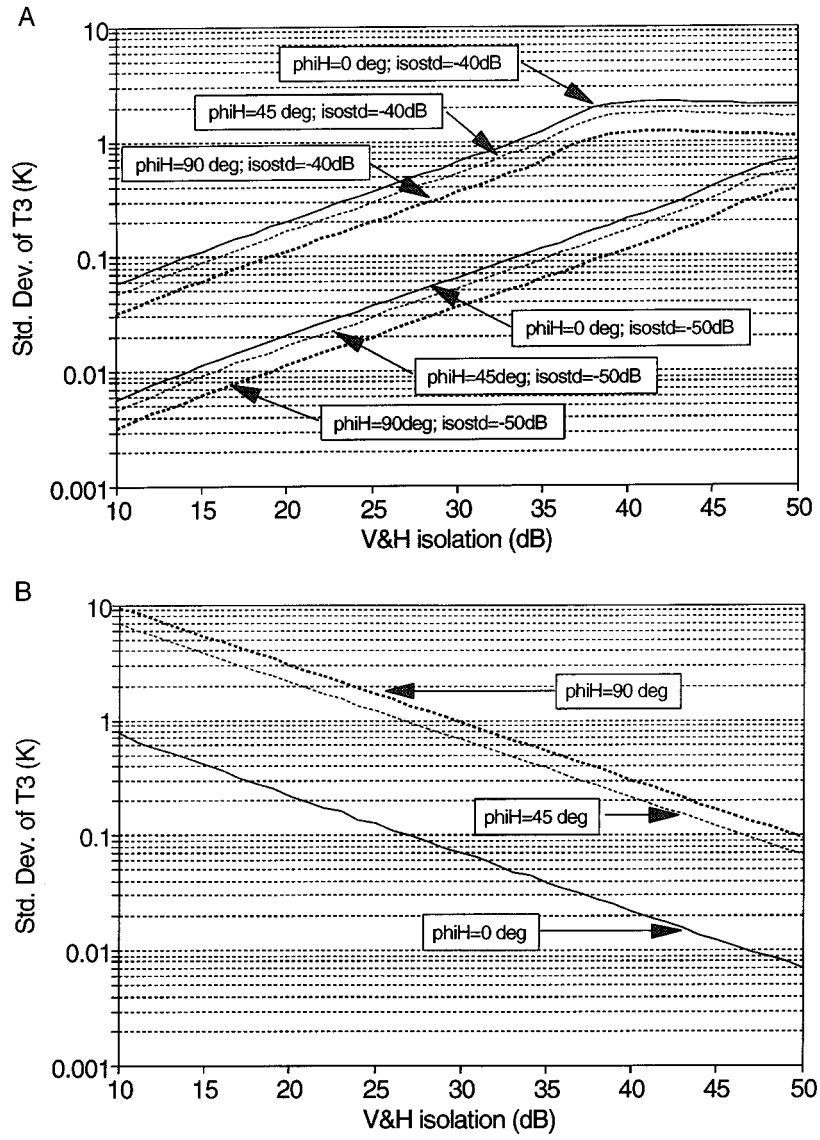

Figure 3. Error in coherent T_3 after instrument corrections are made for the polarization impurity, assuming (a) -40 or -50 dB rms error in knowledge of the isolation between V- and H-pol channels and perfect knowledge of the phase difference between the leakage and the primary signals, and (b) 5° rms error in the relative phase and perfect knowledge of the isolation. Effects of the error in knowledge of the leakage become worse as the isolation improves, until the isolation is comparable to the error itself. The effects of the phase error have an opposite dependence on isolation.

note that σ_{T_3} also depends in a consistent manner on the relative phase of the leakage.

The effects on T_3 calibration of errors in knowledge of the phase of the leakage are considered next. In Figure 3b the phase is assumed known to within $\pm 5°$ rms. The level of leakage is assumed known exactly. The rms error in T_3 is seen to drop monotonically with increasing isolation. This is in marked contrast to the behavior described in Figure 3a, in which the error increases with increasing isolation. In practice, both the level and relative phase of the leakage can never be known exactly. The rms errors in T_3 due to the two causes must, then, be combined (in a root sum squared sense if the two errors are

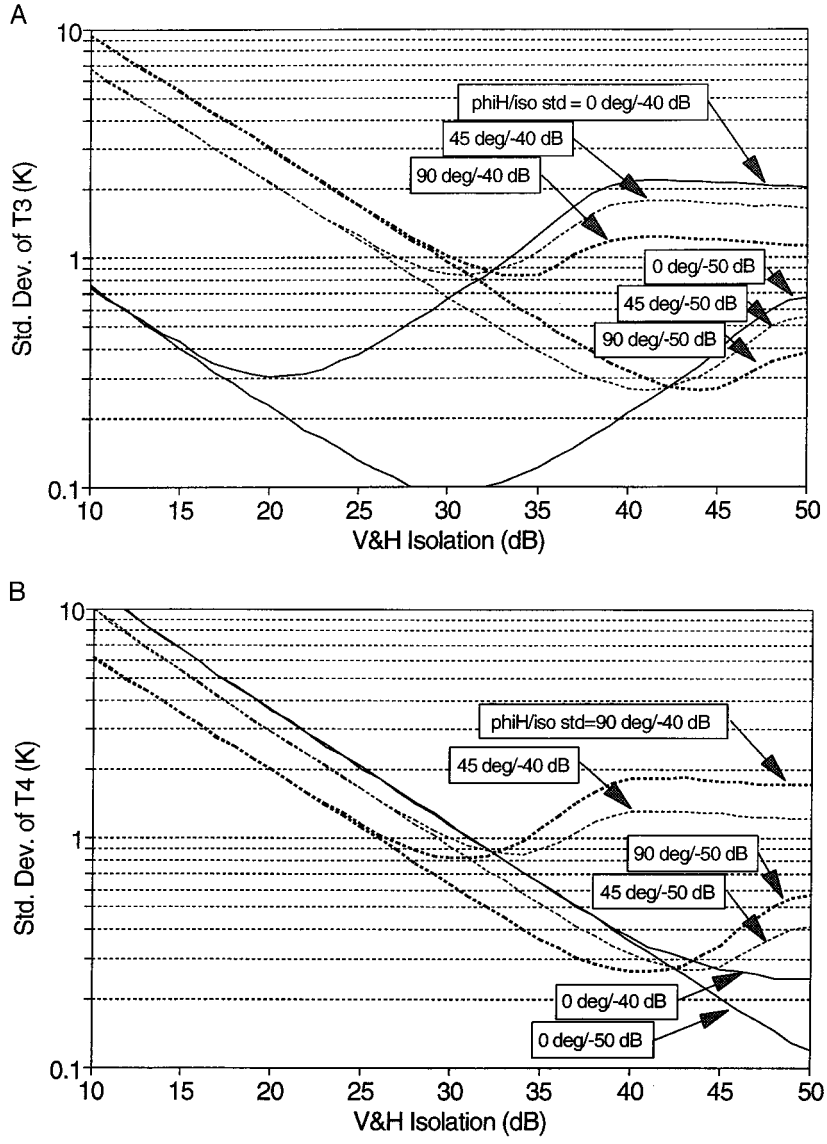

Figure 4. Error in coherent (a) third T_3 and (b) fourth T_4 Stokes parameters after instrument corrections are made, assuming -40 or -50 dB rms error in knowledge of the isolation between V- and H-pol channels and a 5° rms error in knowledge of the phase difference between the leakage and the primary signals. Three nominal phase difference are considered, and the nominal isolation level is varied. Inphase leakage permits T_3 to be much more tolerant of higher levels of leakage.

uncorrelated). The resulting behavior of σ_{T_3} will feature a minimum at some level of leakage where the two competing sources of error are balanced. Note that because of the dependence of σ_{T_3} on the relative phase of the leakage, the location of the minimum will necessarily depend on that phase.

We now consider variations in the level of the isolation, assuming that the errors in knowledge are -40 or -50 dB for the level and 5° for the phase. The resulting standard deviations, σ_{T_3} and σ_{T_4}, of the estimates of the Stokes parameters are shown in Figure 4. Consider first the behavior of σ_{T_3} shown in Figure 4a. It is very sensitive to the relative phase of the V- and H-pol leakage. At the higher levels of leakage (i_V, $i_H < 30$ dB), inphase leakage results in significantly better calibration accuracy. At the very

high levels of leakage (i_V, $i_H < 20$ dB), there is little difference whether errors in knowledge of the leakage are -40 or -50 dB. As the leakage is reduced, however, the -50-dB knowledge becomes clearly superior. At very high isolation (above approximately 40 dB), σ_{T_3} generally becomes insensitive to the level of isolation. This suggests that the calibration error is being dominated by errors in knowledge. This is corroborated by the fact that the -50-dB errors in knowledge have superior calibration there. Finally, note that for inphase leakage the minimum calibration error occurs at a level of isolation roughly 20 dB below the error in knowledge. This general characteristic was pointed out by an anonymous reviewer of this paper.

Comparing σ_{T_4} with σ_{T_3}, one sees there is a marked difference in their behavior with respect to the phase of the leakage. Whereas T_3 is better calibrated provided the leakage is inphase (at the higher levels of leakage), inphase leakage results in the worst calibration of T_4. Calibration of both T_3 and T_4 with 0.4-K accuracy could be problematic, unless errors in knowledge are kept quite low.

We next consider variations of the error in knowledge of the isolation. This might correspond in a spaceborne instrument, for example, to constraints on the allowable drift in isolation over the lifetime of the mission or to constraints on the required accuracy of prelaunch determination of the isolation. For this simulation the level of isolation is fixed at 30 dB, and error in knowledge of the V- and H-pol leakage phase is fixed at 5°. The results are shown in Figure 5. In the case of T_3, calibration accuracy of $\leq$0.4 K requires knowledge at or better than -42 dB with inphase leakage. With other phase differences, even greater knowledge is needed. For T_4 we have already seen from Figure 3 that isolation better than 39 dB is necessary to achieve 0.4-K accuracy. This is corroborated by the results in Figure 5b.

Variations in the error in knowledge of the phase of the leakage signals are considered next. This error might correspond to the allowable drift in or the measurement accuracy of the phase of the leakage. The isolation level is fixed at 30 dB, and error in knowledge of that level is set at -40 dB. The results are shown in Figure 6. In all cases, σ_{T_3} and σ_{T_4} rise with increasing error. The rate of increase varies significantly with the relative phase of the leakage in the case of T_3 and varies less so for T_4. For T_3 the -40-dB error in knowledge of the isolation level dominates the calibration accuracy when the leakage is inphase between channels, preventing it from ever reaching 0.4 K. For a relative phase of 90° the isolation error is less dominant, and a phase accuracy of 1° (which is quite high) manages to bring σ_{T_3} down to 0.4 K. On the other hand, 0.4-K degradation in the accuracy of T_4 occurs with phase errors near 2° at a relative phase of 0°.

4.2. Incoherent Detection of T_3

Because the incoherent detections of T_3 and T_4 are performed by different hardware components, they will be considered separately. Calibration inaccuracies in T_3 are caused by the leakage characteristics of the $\pm$45° channels. In a manner similar to Figure 3 we first consider the individual effects on T_3 calibration of errors in knowledge, while varying the level of the isolation between P- and M-pol channels along with the relative phase of the leakage. Errors in knowledge of the level of the leakage are fixed at -40 or -50 dB, and errors in knowledge of the phase are fixed at 5°, for both channels. The results are shown in Figure 7. The general shape of σ_{T_3} is similar in Figures 3a and 7a, except that in Figure 7a the dependence of σ_{T_3} on the phase of the leakage is not significant. Figures 3b and 7b are also very similar in shape. Note, however, that in both cases the level of the error is significantly lower using incoherent detection.

The superior robustness to errors in knowledge of the hardware characteristics on the part of $T_{3_{inc}}$ relative to $T_{3_{coh}}$ shows up in this and in subsequent parametric studies presented below. It is largely the result of an important difference between the coherent mapping given by (15) and the incoherent relationship given by (17). In the coherent case the dependence of T'_3 on T_V and T_H is through scale factors

$$2 \cos \phi_H \sqrt{i_H/[(1 + i_V)(1 + i_H)]}$$

$$2 \cos \phi_V \sqrt{i_V/[(1 + i_V)(1 + i_H)]},$$

respectively. Increases in either i_V or i_H will result in higher leakage of T_V or T_H into T'_3. The magnitudes of T_V and T_H greatly exceed those of either T_3 or T_4, and so errors in the correction for this leakage will tend to dominate the inversion of (19). In the incoherent case, on the other hand, the T_V and T_H scale factors consist of differences between similar functions of the P- and M-pol isolation. Therefore mutual increases in i_P and i_M will tend to cancel one another out. This fortuitous cancelation effect is a result of the

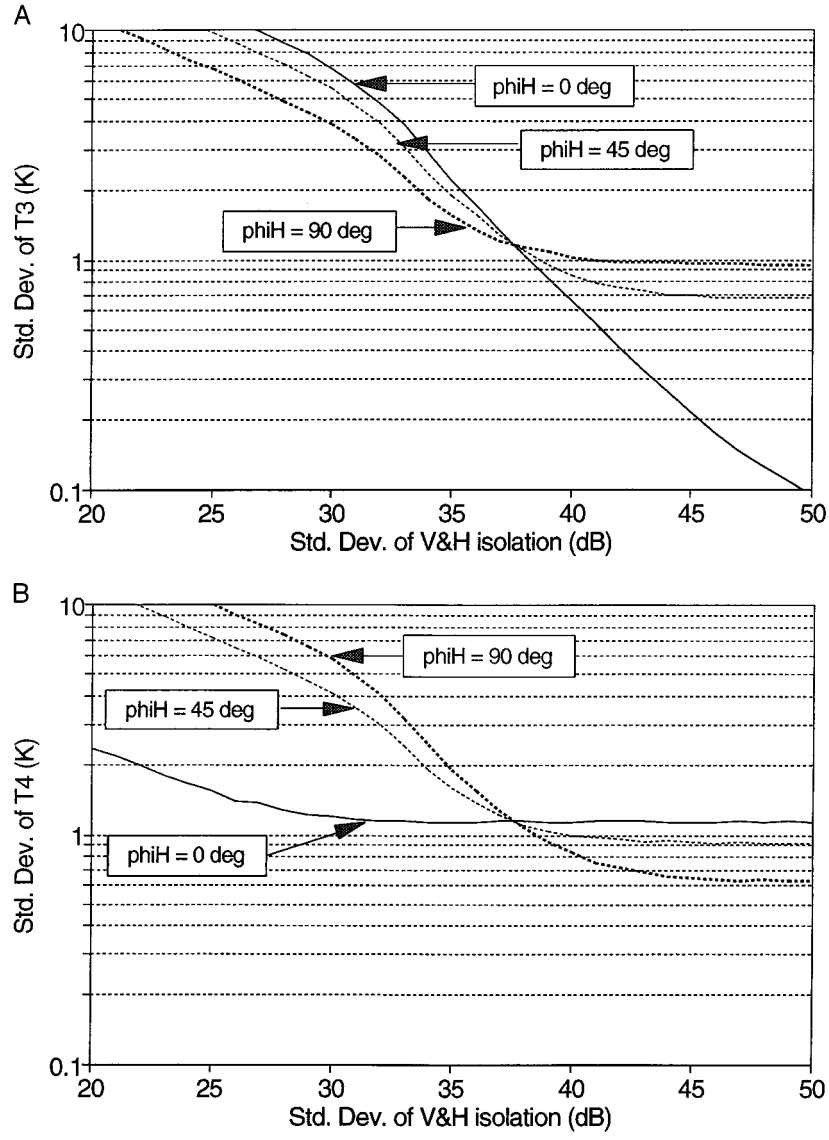

Figure 5. Error in coherent (a) T_3 and (b) T_4, assuming 30-dB isolation between V- and H-pol channels and 5° rms error in knowledge of the leakage phase. Three nominal phase difference are considered, and the error in knowledge of the isolation is varied. Inphase leakage benefits T_4. However, T_3 accuracy of 0.4 K will require isolation knowledge of −42 dB.

differencing scheme used in incoherent detection. Even for the case of unequal isolation ($i_P \neq i_M$), there is still significant partial cancelation. As an example, the incoherent detection error, $T'_{3_{inc}} - T_3$, is shown in Figure 8 for varying degrees of unequal isolation. $T'_{3_{inc}} - T_3$ is small when the P- and M-pol channels are balanced, which suggests that the necessary corrections to T'_3 will be less susceptible to error. (The exact values of i_P and i_M at which $T'_{3_{inc}} - T_3$ is zero are close to, but not exactly, $i_P = i_M$ because of the small contributions to $T'_{3_{inc}}$ from other terms in (17).) Even when the channels are significantly imbalanced, however, the detection error is still well below the coherent case shown in Figure 2a. For example, $i_P = 20$ dB together with $i_M = 30$ dB gives $T'_{3_{inc}} - T_3 = -5$ K. In contrast, $i_V = i_H = 20$ dB gives $T'_{3_{coh}} - T_3 = 60$ K, and $i_V = i_H = 30$ dB gives $T'_{3_{coh}} - T_3 = 15$ K. The contamination of T'_3 is generally much larger in

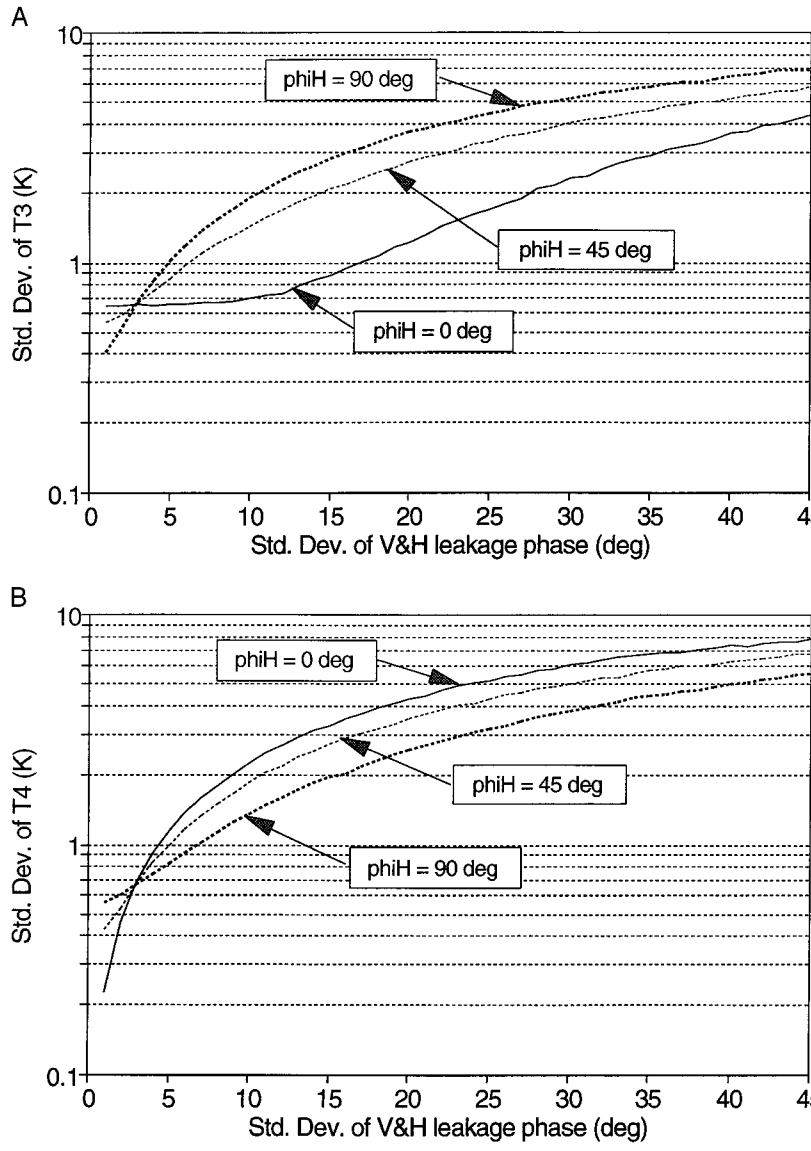

Figure 6. Error in coherent (a) T_3 and (b) T_4, assuming 30-dB isolation between V- and H-pol channels and −40-dB rms error in knowledge of the isolation. Three nominal phase difference are considered, and the error in knowledge of the leakage phase is varied.

the coherent case and so is more prone to errors in the calibration process.

Figure 9 considers errors in knowledge of both the isolation and the relative phase of the leakage, as functions of the level of isolation (Figure 9a), the error in knowledge of the isolation (Figure 9b), and the error in knowledge of the phase (Figure 9c). In Figure 9a the dependence of σ_{T_3} on isolation level, knowledge, and phase has the same general shape as in the coherent case (see Figure 4a). However, the magnitude of the calibration error is significantly lower in the incoherent case. For example, isolation of ~23 dB or better is sufficient to ensure calibration errors of ≤0.4 K at any relative phase or level of knowledge. In the coherent case, only certain combinations of isolation and phase difference perform as well.

Calibration inaccuracies in T_3 due to errors in knowledge of the level and phase of the leakage between P- and M-pol channels are shown in Figures

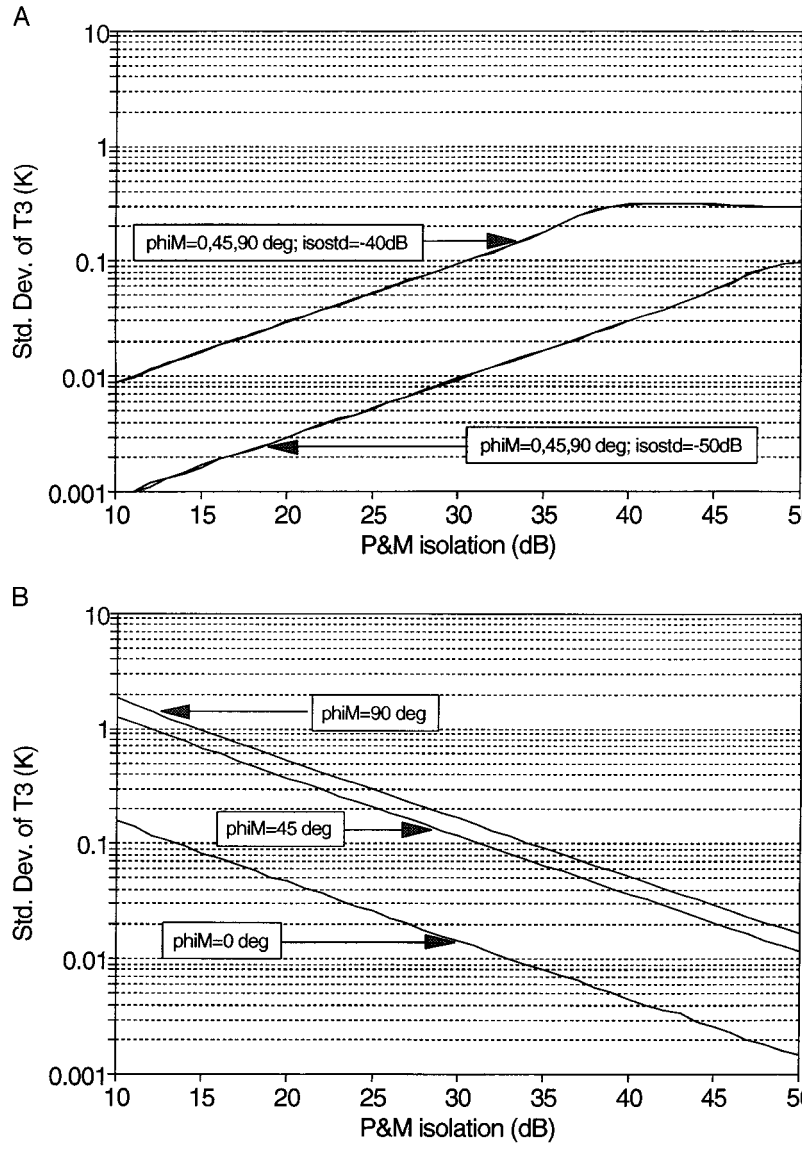

Figure 7. Error in incoherent T_3 after instrument corrections are made for the polarization impurity, assuming (a) -40 or -50 dB rms error in knowledge of the isolation between $\pm 45°$ polarization (P- and M-pol) channels and perfect knowledge of the phase difference between the leakage and the primary signals, and (b) 5° rms error in the relative phase and perfect knowledge of the isolation. Effects of the error in knowledge of the leakage become worse as the isolation improves, until the isolation is comparable to the error itself. The effects of the phase error have an opposite dependence on isolation.

9b and 9c. In both cases the isolation is fixed at 30 dB. Figure 9b varies the error in knowledge of the isolation, with the phase error fixed at 5°. It should be compared with Figure 5a for the equivalent coherent parametric study. The incoherent approach is again more tolerant of errors. For example, assuming in-phase leakage, the level of accuracy achieved in the coherent case with an error of -42 dB ($\sigma_{T_3} = 0.4$ K) is possible in the incoherent case with an error of -36 dB. In other words, the hardware can drift out of calibration 4 times as far in the incoherent case without significantly degrading the retrieval of wind direction. Figure 9c varies the error in knowledge of the phase of the leakage signal, with the error in

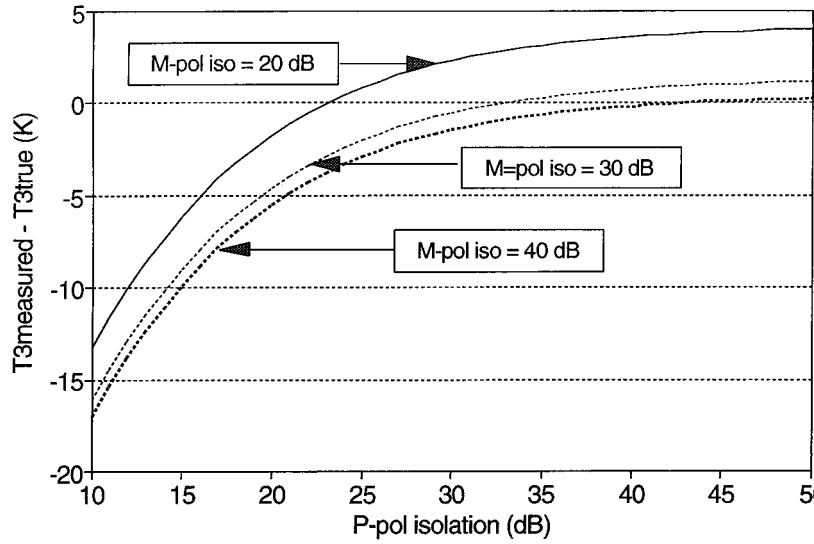

Figure 8. Contamination of the true third Stokes parameter T_3 by polarization impurities in the antenna subsystem, assuming incoherent detection with a variable imbalance between the P- and M-pol levels of isolation. When the isolation is nearly balanced, most of the effects of polarization impurity are canceled out by the differencing operation, T_P–T_M, used to derive T_3. Thus the calibration error resulting from inexact correction for the contamination is smaller near the balanced state. The small residual contamination present when the isolation is balanced results from other terms present in equation (17).

knowledge of the isolation fixed at −40 dB. The comparable coherent case in shown in Figure 6a. The coherent calibration accuracy cannot achieve a $\sigma_{T_3} \leq$ 0.4 K level for any level of phase error, except at a relative phase of 90°. In the incoherent case, $\sigma_{T_3} \leq$ 0.4 K is achieved with all relative phases if the phase error is ≤12°. If the leakage is inphase, then the allowable error in phase knowledge can be relaxed to ≤27°. Overall, it should be emphasized that cases in which the P- and M-pol leakage are inphase are generally less susceptible to calibration inaccuracies. The exception to this is Figure 9b, in which there is a small increase in σ_{T_3} due to errors in knowledge of the level of isolation for inphase leakage.

4.3. Incoherent Detection of T_4

Incoherent detection of T_4 is derived from T_L and T_R according to (9). Our simulations have found it to be particularly insensitive to the level and phase of eccentricity in the L- and R-pol channels. For example, parametric studies which independently varied the levels of eccentricity, e_L and e_R, while fixing $\phi_L = \phi_R = 0°$ and fixing the error in knowledge of the eccentricity at −40 dB and in knowledge of the phase at 5°, found no significant effect on σ_{T_4}. Similarly, independent variations of ϕ_L and ϕ_R over ±20° (with $e_L = e_R = 1$ and the same errors in knowledge) found little effect on σ_{T_4}. In other words, the exact circularity of the L- and R-pol channels is much less important than how well its eccentricity is known. Parametric variations in the errors in knowledge corroborate this. The sensitivity of calibration accuracy to errors in knowledge of e_L and e_R (fixing $\phi_L = \phi_R = 0°$ and error in knowledge of the phase at 5°) is shown in Figure 10a. Note that σ_{T_4} is essentially the same for all e_L and e_R between 0.9 and 1.1, as noted above. Knowledge of the eccentricity to better than −17 dB provides $\sigma_{T_4} \leq$ 0.4 K. Below −25 dB, σ_{T_4} does not decrease significantly with improved knowledge of the eccentricity. This indicates that σ_{T_4} is dominated by the 5° phase error. Figure 10b shows the calibration sensitivity to errors in knowledge of ϕ_L and ϕ_R, fixing $e_L = e_R = 1.0$, $\phi_L = \phi_R = 0°$, and errors in knowledge of e_L and e_R at −40 dB. From the figure, σ_{T_4} equals 0.4 K for a phase uncertainty of approximately 13° and continues to drop as phase uncertainty is reduced, indicating that errors in phase dominate σ_{T_4}.

The relative sensitivities to calibration errors in coherent and incoherent detection of T_4 can be seen by comparing Figure 10 with Figures 5b and 6b. In the

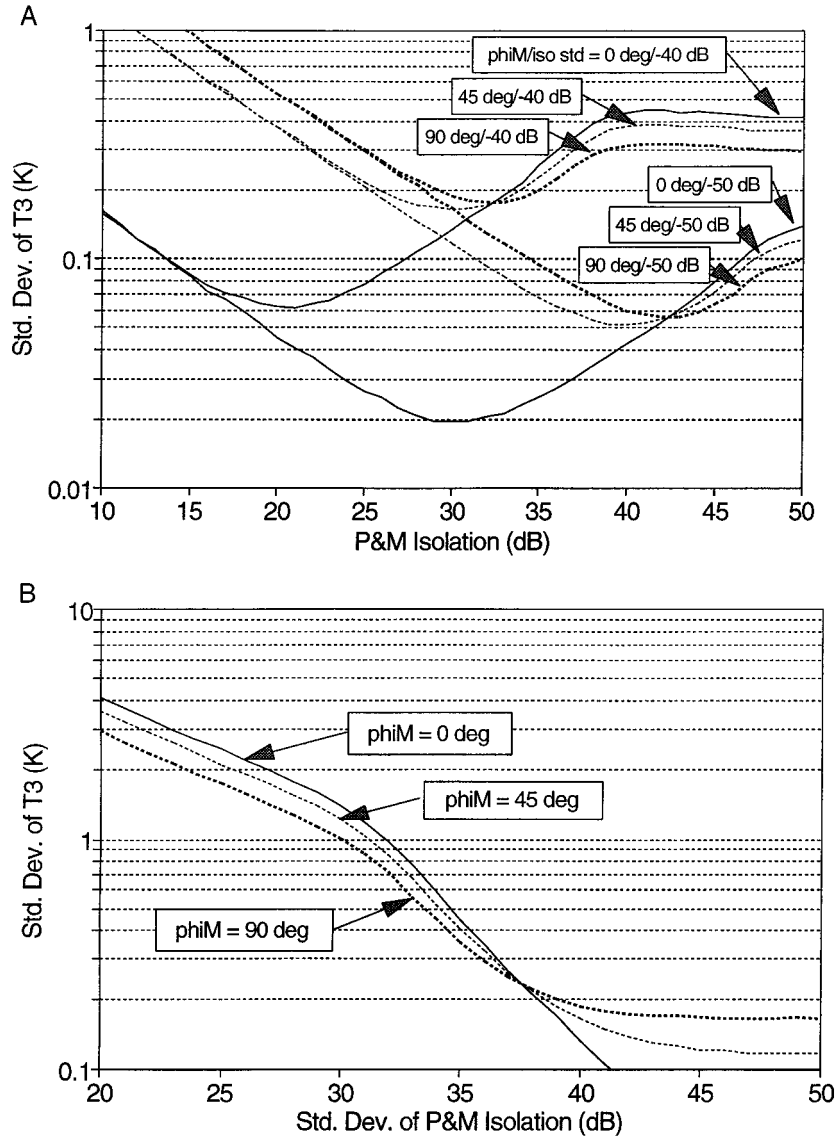

Figure 9. Error in incoherent T_3 due to inexact hardware corrections (a) assuming -40 or -50 dB rms error in knowledge of the isolation between P- and M-pol channels and a 5° rms error in knowledge of the phase difference between the leakage and the primary signals (P- and M-pol isolation is varied); (b) assuming 30-dB isolation between P- and M-pol channels and 5° rms error in knowledge of the leakage phase (knowledge of the isolation is varied); and (c) assuming 30-dB isolation between P- and M-pol channels and -40-dB rms error in knowledge of the isolation (knowledge of the leakage phase is varied). With inphase leakage, T_3 accuracy of 0.4 K requires 10-dB isolation, 36-dB isolation knowledge, or 27° phase knowledge. The more tolerant incoherent requirements result from fortuitous cancelation of the calibration errors in the T_P–T_M differencing operation.

coherent case, V- and H-pol isolation plays a role similar to e_L and e_R in the incoherent case. From Figure 5b, errors significantly larger than 0.4 K are present at all levels of error in knowledge of i_V and i_H. This is in contrast to the incoherent case, in which a -17-dB requirement on knowledge of e_L and e_R is sufficient to provide a calibration error of 0.4 K. From Figure 6b we see that phase uncertainties of as little as 1° in the coherent detection of T_4 are still insufficiently accurate to provide a calibration error of $\leq$0.4

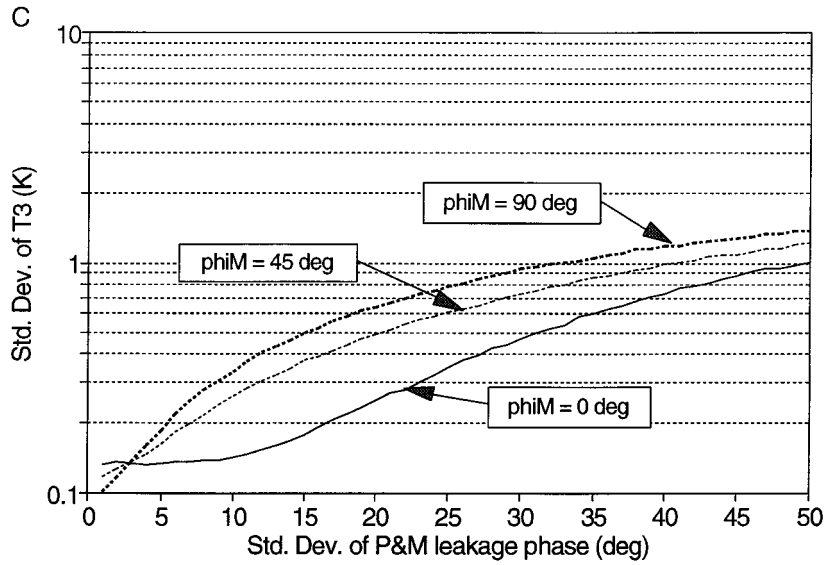

Figure 9. (continued)

K. In the incoherent case, on the other hand, a phase uncertainty of 13° is sufficient. The fact that incoherent estimation of T_4 using (9) is more forgiving of hardware uncertainties results from the differencing scheme, $T_L - T_R$. Just as in the case of $T_{3_{inc}}$ described above, there is significant cancelation of the nonideal hardware characteristics inherent in the relationship, equation (18), between $T'_{4_{inc}}$ and T_V and T_H.

5. Precision of Stokes Measurements

The four element vector measurements, $\mathbf{T}'_{coh}$ and $\mathbf{T}'_{inc}$, will be corrupted by zero mean additive Gaussian noise. In the coherent case we assume that each of the four measurements has uncorrelated noise with the same standard deviation, ΔT. This neglects possible degradation in the signal-to-noise ratio from the cross correlator, for example, due to quantization and/or undersampling [*Hagen and Farley*, 1973], by assuming that a sufficient number of bits and clock speed are used. The coherent measurement covariance is then given by

$$\Gamma'_{coh} = \Delta T^2 I \tag{21}$$

where I is the identity matrix. Inversion of (19), to estimate T_3 and T_4, will result in a modified covariance, Γ_{coh}, for the estimated third and fourth Stokes parameters given by

$$\Gamma_{coh} = \mathbf{R}_{coh}^{-1}\Gamma'_{coh}(\mathbf{R}_{coh}^{-1})^{\dagger} \tag{22}$$

where the dagger denotes the matrix transpose. The square roots of the third and fourth main diagonal elements of Γ_{coh} give the resulting precision of the estimates of T_3 and T_4. The ratios $\sqrt{\Gamma_{coh}(3,3)}/\Delta T$ and $\sqrt{\Gamma_{coh}(4,4)}/\Delta T$ give the noise multiplication factors (NMFs) of the measurement ΔT due to the inversion. These ratios are plotted in Figure 11 as functions of the V- and H-channel isolation and the relative phase of the leakage signals. The NMF is at or near unity for isolation levels of ~20 dB or better at all relative phases of the leakage and for both T_3 and T_4. In a properly designed radiometer, in which the accuracy considerations described above are adequately addressed, this level of isolation would likely be present anyway.

For the incoherent case, T'_3 and T'_4 will have twice the variance of the coherent measurements, or of T'_V and T'_H, because of (8) and (9). For this reason, the measurement covariance will be diagonal, with main diagonal elements given by

$$\Gamma'_{inc}(i,i) = \begin{cases} \Delta T^2 & i = 1, 2 \\ 2\Delta T^2 & i = 3, 4 \end{cases} \tag{23}$$

Inversion of (20) gives the incoherent covariance, Γ_{coh}, for the estimated Stokes parameters as

$$\Gamma_{inc} = \mathbf{R}_{inc}^{-1}\Gamma'_{inc}(\mathbf{R}_{inc}^{-1})^{\dagger} \tag{24}$$

The NMFs, $\sqrt{\Gamma_{inc}(3,3)}/\Delta T$ and $\sqrt{\Gamma_{inc}(4,4)}/\Delta T$, for T_3 and T_4 are shown in Figure 12 as functions of

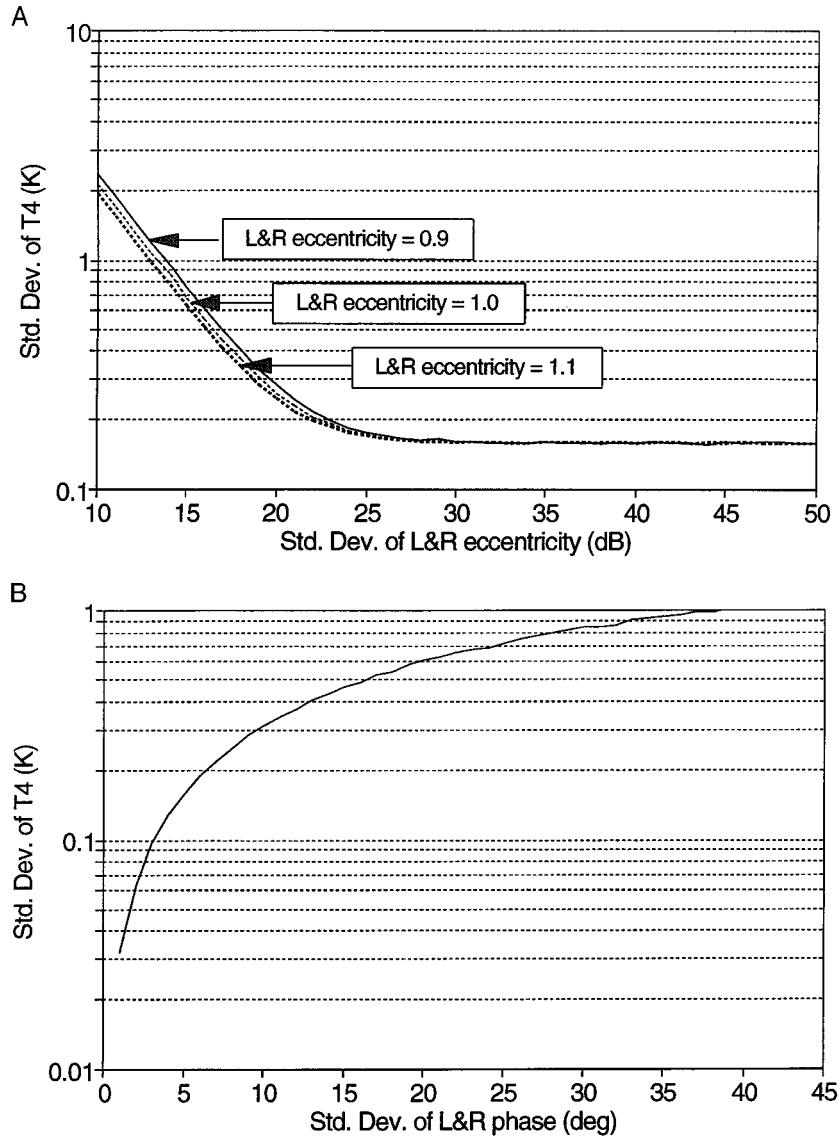

Figure 10. Error in incoherent T_4 due to inexact hardware corrections (a) assuming a nominal 90° phase difference between V- and H-pol components of the LHCP and RHCP channels and assuming 5° rms error in knowledge of the true phase difference (knowledge of the LHCP and RHCP eccentricity is varied), and (b) assuming nominal eccentricity of 1.0 and −40-dB error in knowledge of the eccentricity (knowledge of the nominal 90° phase difference between V- and H-pol components is varied).

appropriate hardware parameters. For T_3 the NMF increases as the P- and M-channel isolation drops, in a manner similar to the coherent case. The higher $(2\Delta T^2)$ initial variance for T'_3 results in a lowest achievable NMF of $\sqrt{2}$. This level is reached for isolation values at or above ~20 dB, similar to the coherent case.

The dependence of the $T_{4_{\text{inc}}}$ NMF on eccentricity is shown in Figure 12b. The lowest achievable NMF (of $\sqrt{2}$) occurs for the ideal case $e_{\text{L}} = e_{\text{R}} = 1$. At other levels of eccentricity, including cases with significant imbalance between the L- and R-pol channels, the increase in NMF is extremely gradual and would not be considered significant in most applications.

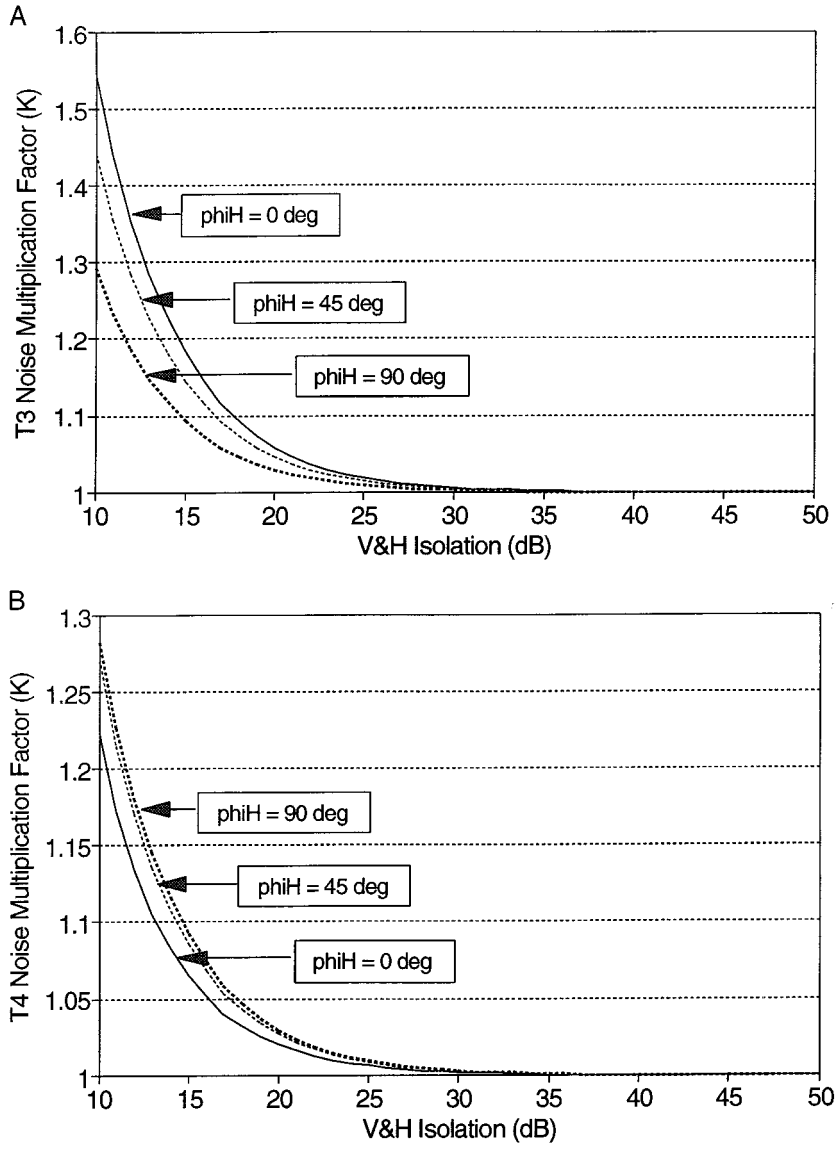

Figure 11. Multiplicative effect on ΔT noise of hardware corrections to coherent (a) T_3 and (b) T_4 measurements. Minimal noise amplification results, provided the V- and H-pol isolation is $\geq$20 dB.

6. Implications on Instrument Design and Testing

The results presented here suggest several guidelines concerning performance requirements of the antenna subsystem in a polarimetric radiometer. The antenna subsystem is taken here to include all passive components, such as a main reflector, feed horn, orthomode transducer, and $\pm 180°$ and $\pm 90°$ hybrids, that can influence the level of cross talk between the true Stokes parameters and the actual measurements. These guidelines fall into the two general categories of nominal hardware specifications and knowledge of exact hardware performance. The first category would influence the initial part and subsystem specifications for the antenna, for example, the isolation or eccentricity must be at or better than a certain level, or the phase difference between the primary and orthogonal leakage signals must be within so many degrees of a certain value. The second category influences a number of design and calibration issues.

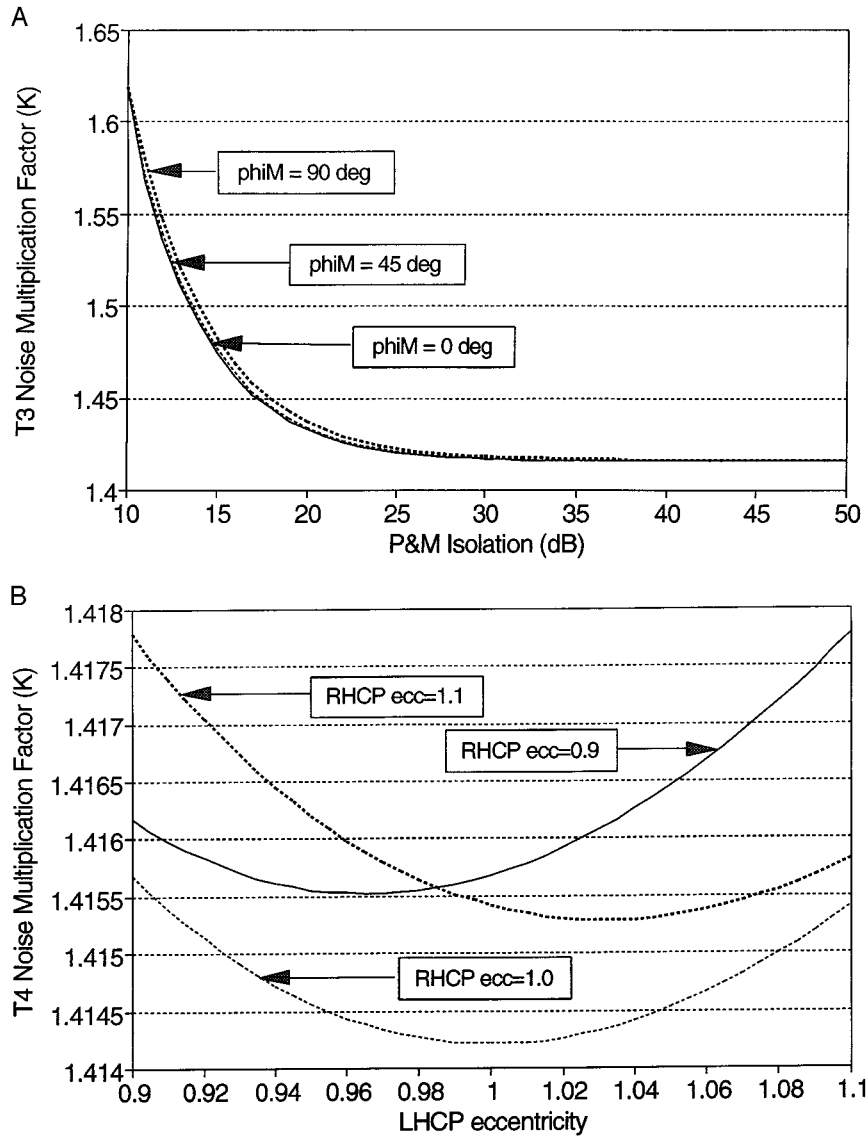

Figure 12. Multiplicative effect on ΔT noise of hardware corrections to incoherent measurements. (a) For T_3, very high isolation guarantees a "best possible" noise level of $\sqrt{2}\Delta T$, due to the differencing operations needed. Isolation above 20 dB would, in most cases, be sufficient. (b) For T_4, balanced unity eccentricity for the LHCP and RHCP channels results in a $\sqrt{2}\Delta T$ noise level. However, imbalanced eccentricities suffer a negligible increase in noise.

Initially, a "knowledge" requirement defines how well a certain specification must be measured. Later, it defines how much that specification can be allowed to drift. Thus the knowledge requirement might also influence initial part selection since, for example, an antenna with slightly poorer cross-polarization isolation may be inherently much more stable.

For radiometers using coherent detection, there are two competing components of calibration error that affect the required isolation. Errors due to inexact knowledge of the level of leakage tend to increase as isolation improves. Errors due to knowledge of the phase of the leakage will decrease with improving isolation. The optimum level of isolation, at which the calibration error is a minimum, will vary according to the nominal phase of the leakage and

according to the errors in knowledge. For example, if the nominal isolation between the V- and H-pol channels is relatively poor (in the vicinity of 20 dB) but is known to −40 dB (i.e., is known to one part in a hundred), then the error in calibration of T_3 is considerably aided if the relative phase of the leakage is 0°. This assumes that the relative phase is known to 5°. If, on the other hand, the nominal isolation is quite high (in the vicinity of 40 dB), then a 90° phase difference will provide better calibration. In all cases, lower errors in knowledge of either the phase or level of the leakage will result in improved calibration. However, the degree to which the lower errors help will depend on the nominal isolation. This relationship may provide a meaningful cost/benefit trade-off in terms of the possible diminishing returns of very high levels of knowledge. It should also be noted that, in general, the optimum level of isolation and relative phase of the leakage for T_4 calibration is not consistent with that for T_3. In many of the parametric cases considered, a significant compromise must be made in the calibration accuracy of one in order to optimize the calibration of the other.

For incoherent detection of T_3 the same competing components of error exist as in the coherent case. The result is an optimum level of isolation between the P- and M-pol channels, which varies with the relative phase of the leakage and with the errors in knowledge of both the leakage phase and level. In the incoherent case, however, the magnitude of the resulting calibration error can be much lower. For example, P- and M-pol isolation of 20 dB with −40-dB knowledge and inphase leakage with 5° knowledge results in a calibration error of 0.06 K. The error in coherent detection of T_3 under comparable conditions is 0.3 K.

One special case of cross-polarization leakage deserves particular attention. As mentioned above, a physical rotation of the antenna about its main-beam axis will result in balanced isolation levels ($i_V = i_H = i_P = i_M = (\sin\theta/\cos\theta)^2$, where θ is the rotation angle). If the calibration mapping $\mathbf{R}^{-1}$ knows a priori that the leakage is balanced, then while there may be errors in knowledge of the level of isolation, there will be no error in knowledge of the difference between i_V and i_H in the coherent case or between i_P and i_M in the incoherent case. In this case, the calibration accuracy of the coherent and incoherent approaches is identical. In the more general case, when the possibility of imbalances in the polarization leakage exists and thus there is an error associated with knowledge of the imbalance, the incoherent approach is significantly less sensitive to those errors.

Incoherent detection of T_4 is relatively insensitive to the level of eccentricity in the RHCP and LHCP channels. Thus an "optimal" level of eccentricity would generally not be an important antenna design constraint. Errors in knowledge of the eccentricity and the phase of the leakage are more important. Reduced errors will result in improved calibration, just as in the other cases considered above.

The final choice between coherent and incoherent approaches to the radiometer design must trade off their respective pros and cons. Most notably, coherent detection requires a single complex correlation channel, and it has the capability for superior performance with respect to precision, provided the correlation is implemented without adding noise. This is principally the result of the differencing operation needed to derive T_3 and T_4 using incoherent detection, which is avoided in the coherent case. Incoherent detection, on the other hand, requires four conventional radiometer channels, but it has the capability for superior performance with respect to absolute accuracy. The effects of small drifts or errors in knowledge of the polarization purity of the data are, to first order, canceled out by the same differencing operation that degraded its precision. Incoherent detection also permits the use of components and subsystems which have less severe performance requirements with regard to isolation and phase balance.

Appendix: Development of Instrument Measurement Model

The relationship between a partially polarized electric field incident on a microwave radiometer's antenna and the detected output measured by the radiometer can be readily explained using the concept of a vector complex effective antenna height, $\hat{a}$ [*Ishimaru*, 1991]. Let the incident electric field be given by

$$\mathbf{E} = E_V\hat{V} + E_H\hat{H} \tag{A1}$$

where $\hat{V}$ and $\hat{H}$ are unit vectors in the vertical and horizontal directions, respectively. Ideal antenna heights for antenna polarizations of interest in polarimetric radiometry are

$$\text{Vertical polarization} \qquad \hat{a}^{V}_{\text{ideal}} = \hat{V} \tag{A2}$$

Horizontal polarization $\hat{a}^{\mathrm{H}}_{\mathrm{ideal}} = \hat{H}$ (A3)

+45° linear polarization $\hat{a}^{\mathrm{P}}_{\mathrm{ideal}} = (\hat{V} + \hat{H})/\sqrt{2}$ (A4)

−45° linear polarization $\hat{a}^{\mathrm{M}}_{\mathrm{ideal}} = (\hat{V} - \hat{H})/\sqrt{2}$ (A5)

Left-hand circular polarization

$$\hat{a}^{\mathrm{L}}_{\mathrm{ideal}} = (\hat{H} - j\hat{V})/\sqrt{2} \tag{A6}$$

Right-hand circular polarization

$$\hat{a}^{\mathrm{R}}_{\mathrm{ideal}} = (\hat{H} + j\hat{V})/\sqrt{2} \tag{A7}$$

The ideal detected measurements by the radiometer are

$$T_{\mathrm{V}} = c\langle|\hat{a}^{\mathrm{V}}_{\mathrm{ideal}}\cdot\mathbf{E}|^2\rangle = c\langle|E_{\mathrm{V}}|^2\rangle \tag{A8}$$

$$T_{\mathrm{H}} = c\langle|\hat{a}^{\mathrm{H}}_{\mathrm{ideal}}\cdot\mathbf{E}|^2\rangle = c\langle|E_{\mathrm{H}}|^2\rangle \tag{A9}$$

$$T_{\mathrm{P}} = c\langle|\hat{a}^{\mathrm{P}}_{\mathrm{ideal}}\cdot\mathbf{E}|^2\rangle = c\left[\frac{\langle|E_{\mathrm{V}}|^2\rangle + \langle|E_{\mathrm{H}}|^2\rangle}{2} + \mathrm{Re}\,\{\langle|E_{\mathrm{V}}E^*_{\mathrm{H}}|\rangle\}\right] \tag{A10}$$

$$T_{\mathrm{M}} = c\langle|\hat{a}^{\mathrm{M}}_{\mathrm{ideal}}\cdot\mathbf{E}|^2\rangle = c\left[\frac{\langle|E_{\mathrm{V}}|^2\rangle + \langle|E_{\mathrm{H}}|^2\rangle}{2} - \mathrm{Re}\,\{\langle|E_{\mathrm{V}}E^*_{\mathrm{H}}|\rangle\}\right] \tag{A11}$$

$$T_{\mathrm{L}} = c\langle|\hat{a}^{\mathrm{L}}_{\mathrm{ideal}}\cdot\mathbf{E}|^2\rangle = c\left[\frac{\langle|E_{\mathrm{V}}|^2\rangle + \langle|E_{\mathrm{H}}|^2\rangle}{2} + \mathrm{Im}\,\{\langle|E_{\mathrm{V}}E^*_{\mathrm{H}}|\rangle\}\right] \tag{A12}$$

$$T_{\mathrm{R}} = c\langle|\hat{a}^{\mathrm{R}}_{\mathrm{ideal}}\cdot\mathbf{E}|^2\rangle = c\left[\frac{\langle|E_{\mathrm{V}}|^2\rangle + \langle|E_{\mathrm{H}}|^2\rangle}{2} - \mathrm{Im}\,\{\langle|E_{\mathrm{V}}E^*_{\mathrm{H}}|\rangle\}\right] \tag{A13}$$

where $c = \lambda^2/k\eta B$, where λ is the RF center frequency, k is the Boltzmann constant, η is the intrinsic impedance of free space, and B is the RF bandwidth. Combining (A10)–(A13), incoherent measurement of the third and fourth Stokes parameters follows as

$$T_{3_{\mathrm{inc}}} \equiv T_{\mathrm{P}} - T_{\mathrm{M}} = 2c\ \mathrm{Re}\,\{\langle|E_{\mathrm{V}}E^*_{\mathrm{H}}|\rangle\} \tag{A14}$$

$$T_{4_{\mathrm{inc}}} \equiv T_{\mathrm{L}} - T_{\mathrm{R}} = 2c\ \mathrm{Im}\,\{\langle|E_{\mathrm{V}}E^*_{\mathrm{H}}|\rangle\} \tag{A15}$$

where we have adopted the notation T_3 and T_4, rather than the conventional U and V, to avoid confusion with the vertical coordinate designation, V.

Alternatively, coherent measurement of T_3 and T_4 is accomplished by a direct correlation of E_{V} with E_{H}. Since the dot product of $\hat{a}^{\mathrm{V}}$ ($\hat{a}^{\mathrm{H}}$) with $\mathbf{E}$ represents the component of the incident field leaving the vertical (horizontal) antenna port, this correlation is given by

$$T_{3_{\mathrm{coh}}} \equiv 2c\ \mathrm{Re}\,\{\langle(\hat{a}^{\mathrm{V}}_{\mathrm{ideal}}\cdot\mathbf{E})(\hat{a}^{\mathrm{H}}_{\mathrm{ideal}}\cdot\mathbf{E})^*\rangle\} \tag{A16}$$

$$T_{4_{\mathrm{coh}}} \equiv 2c\ \mathrm{Im}\,\{\langle(\hat{a}^{\mathrm{V}}_{\mathrm{ideal}}\cdot\mathbf{E})(\hat{a}^{\mathrm{H}}_{\mathrm{ideal}}\cdot\mathbf{E})^*\rangle\} \tag{A17}$$

Note that (A16) and (A17) reduce to the right-hand sides of (A14) and (A15), respectively, given ideal antenna characteristics.

In practice, numerous nonideal hardware characteristics contribute to deviations of the true antenna heights from those given by (A2)–(A7). For example, the orthomode transducer typically used on antenna feed horns to separate orthogonal linearly polarized components of the incident field has leakage signals from the unwanted polarization. This can be modeled by a modification to (A2) and (A3) as

$$\hat{a}^{\mathrm{V}} = (\hat{V} + \sqrt{i_{\mathrm{V}}}\hat{H}e^{j\phi_{\mathrm{V}}})/\sqrt{1 + i_{\mathrm{V}}} \tag{A18}$$

$$\hat{a}^{\mathrm{H}} = (\hat{H} + \sqrt{i_{\mathrm{H}}}\hat{V}e^{j\phi_{\mathrm{H}}})/\sqrt{1 + i_{\mathrm{H}}} \tag{A19}$$

where i_{V} (i_{H}) is the isolation at the vertical (horizontal) port from leakage of the horizontal (vertical) signal and ϕ_{V} (ϕ_{H}) is the phase of the horizontal (vertical) signal with respect to the vertical (horizontal) signal leaving the vertical (horizontal) port. Using (A18) in place of (A2) in the relation (A8) for T_{V} gives

$$T'_{\mathrm{V}} = [T_{\mathrm{V}} + i_{\mathrm{V}}T_{\mathrm{H}} + \sqrt{i_{\mathrm{V}}}(T_3\cos\phi_{\mathrm{V}} + T_4\sin\phi_{\mathrm{V}})]/(1 + i_{\mathrm{V}}) \tag{A20}$$

where T'_{V} is the actual brightness temperature that would be detected leaving the vertical antenna port, and T_{V}, T_{H}, T_3, and T_4 are the ideal brightness temperatures given by (A8), (A9), (A14), and (A15). Similarly for T_{H}, using (A19) in place of (A3) in (A9) gives

$$T'_{\mathrm{H}} = [T_{\mathrm{H}} + i_{\mathrm{H}}T_{\mathrm{V}} + \sqrt{i_{\mathrm{H}}}(T_3\cos\phi_{\mathrm{H}} - T_4\sin\phi_{\mathrm{H}})]/(1 + i_{\mathrm{H}}) \tag{A21}$$

Note in both (A20) and (A21) that knowledge of the magnitude of the isolation, i_V or i_H, together with measurements of T'_V and T'_H alone, is insufficient information from which to solve for T_V and T_H. This problem was recognized by *Njoku et al*. [1980] while developing the antenna pattern correction algorithm for the Seasat scanning multichannel microwave radiometer.

Coherent measurements of T_3 and T_4 by a nonideal antenna are determined by using (A18) and (A19) in place of (A2) and (A3) in (A16) and (A17), giving

$$\begin{aligned}(T'_3 + jT'_4)_{coh} &= 2c\{\langle(\hat{a}^V \cdot \mathbf{E})(\hat{a}^H \cdot \mathbf{E})^*\rangle\} \\ &= 2c\{\langle E_V E_H^*\rangle + \langle E_H E_V^*\rangle\sqrt{i_V i_H}e^{j(\phi_V-\phi_H)} + \langle|E_V|^2\rangle\sqrt{i_H}e^{-j\phi_H} \\ &\quad + \langle|E_H|^2\rangle\sqrt{i_V}e^{j\phi_V}\}/\sqrt{(1+i_V)(1+i_H)} \\ &= \{T_3 + jT_4 + (T_3 - jT_4)\sqrt{i_V i_H}e^{j(\phi_V-\phi_H)} \\ &\quad + 2T_V\sqrt{i_H}e^{-j\phi_H} + 2T_H\sqrt{i_V}e^{j\phi_V}\}/\sqrt{(1+i_V)(1+i_H)}\end{aligned} \tag{A22}$$

Separating (A22) into real and imaginary parts gives

$$\begin{aligned}T'_{3_{coh}} &= \{T_3[1 + \sqrt{i_V i_H}\cos(\phi_V - \phi_H)] \\ &\quad + T_4\sqrt{i_V i_H}\sin(\phi_V - \phi_H) + 2T_V\sqrt{i_H}\cos\phi_H \\ &\quad + 2T_H\sqrt{i_V}\cos\phi_V\}/\sqrt{(1+i_V)(1+i_H)}\end{aligned} \tag{A23}$$

$$\begin{aligned}T'_{4_{coh}} &= \{T_4[1 - \sqrt{i_V i_H}\cos(\phi_V - \phi_H)] \\ &\quad + T_3\sqrt{i_V i_H}\sin(\phi_V - \phi_H) - 2T_V\sqrt{i_H}\sin\phi_H \\ &\quad + 2T_H\sqrt{i_V}\sin\phi_V\}/\sqrt{(1+i_V)(1+i_H)}\end{aligned} \tag{A24}$$

Note in (A23) and (A24) that nonideal measurements, T'_3 and T'_4, are corrupted by a fraction of T_V and T_H. T_V and T_H are often several orders of magnitude greater than either T_3 or T_4 [*Wilson and Yueh*, 1996], so this leakage can have a serious negative impact on calibration accuracy if it is corrected improperly.

The ±45° linear polarization channels will also suffer nonideal leakage between orthogonal components. One convenient way to form the slant linear polarizations is by combining the V and H outputs using 0° and 180° hybrids [*Yueh et al*., 1995]. Assuming ideal phase and amplitude balancing of these hybrids, but nonideal V and H characteristics of the antenna itself, the resulting effective antenna heights would be $\hat{a}^{P/M} = (\hat{a}^V \pm \hat{a}^H)/\sqrt{2}$. In practice, however, it may be no more accurate to assume ideal hybrids than ideal antenna isolation. For this reason, we adopt a more general expression for the effective height that is composed of a desired colinear component and an orthogonal leakage term given by

$$\hat{a}^P = (\hat{a}^P_{ideal} + \sqrt{i_P}\hat{a}^M_{ideal}e^{j\phi_P})/\sqrt{1+i_P} \tag{A25}$$

$$\hat{a}^M = (\hat{a}^M_{ideal} + \sqrt{i_M}\hat{a}^P_{ideal}e^{j\phi_M})/\sqrt{1+i_M} \tag{A26}$$

where $i_P(i_M)$ is the isolation at the +45° (−45°) port from leakage of the −45° (+45°) signal and ϕ_P (ϕ_M) is the phase of the −45° (+45°) signal with respect to the +45° (−45°) signal leaving the +45° (−45°) port. Using (A25) in place of (A4) in the relation (A10) for T_P gives

$$\begin{aligned}T'_P &= [T_V(1 + 2\sqrt{i_P}\cos\phi_P + i_P) \\ &\quad + T_H(1 - 2\sqrt{i_P}\cos\phi_P + i_P) \\ &\quad + T_3(1 - i_P) - 2T_4\sqrt{i_P}\sin\phi_P]/[2(1+i_P)]\end{aligned} \tag{A27}$$

and similarly replacing (A5) by (A26) in (A11) for T_M gives

$$\begin{aligned}T'_M &= [T_V(1 + 2\sqrt{i_M}\cos\phi_M + i_M) \\ &\quad + T_H(1 - 2\sqrt{i_M}\cos\phi_M + i_M) - T_3(1 - i_M) \\ &\quad + 2T_4\sqrt{i_M}\sin\phi_M]/[2(1+i_M)]\end{aligned} \tag{A28}$$

where $T'_{P/M}$ are the actual brightness temperatures that would be detected leaving the ±45° hybrid ports. Note that $i_P = i_M = 0$ gives $T'_{P/M} = (T_V + T_H \pm T_3)/2$.

Incoherent measurement of T_3 by a nonideal antenna and hybrid is determined by using (A27) and (A28) in place of (A10) and (A11) in (A14), giving

$$\begin{aligned}T'_{3_{inc}} &\equiv T'_P - T'_M = T_V[(1 + 2\sqrt{i_P}\cos\phi_P + i_P)/(1+i_P) \\ &\quad - (1 + 2\sqrt{i_M}\cos\phi_M + i_M)/(1+i_M)]/2 \\ &\quad + T_H[(1 - 2\sqrt{i_P}\cos\phi_P + i_P)/(1+i_P) \\ &\quad - (1 - 2\sqrt{i_M}\cos\phi_M + i_M)/(1+i_M)]/2 \\ &\quad + T_3[(1 - i_P)/(1+i_P) + (1 - i_M)/(1+i_M)]/2 \\ &\quad - T_4[\sqrt{i_P}\sin\phi_P/(1+i_P) + \sqrt{i_M}\sin\phi_M/(1+i_M)]\end{aligned} \tag{A29}$$

Note that as in (A23), $T'_{3_{inc}}$ is also corrupted by a fraction of T_V and T_H.

The left- and right-hand circular polarization (LHCP and RHCP) channels will, in general, also be nonideal. T_L and T_R can be formed by combining the V and H outputs using a $\pm 90°$ quadrature [*Yueh et al.*, 1995]. If the quadrature hybrid is ideal, the resulting effective antenna heights are $\hat{a}^{R/L} = (\hat{a}^H \pm j\hat{a}^V)/\sqrt{2}$. Because of nonideal behavior by the hybrid, we adopt a more general elliptically polarized expression given by

$$\hat{a}^L = (\sqrt{e_L}\hat{H} - j\hat{V}e^{j\phi_L})/\sqrt{1 + e_L} \tag{A30}$$

$$\hat{a}^R = (\sqrt{e_R}\hat{H} + j\hat{V}e^{j\phi_R})/\sqrt{1 + e_R} \tag{A31}$$

where e_L (e_R) is the eccentricity of the LHCP (RHCP) channel, defined as the ratio of sensitivity to horizontal versus vertical polarized signals and where ϕ_L (ϕ_R) is the phase deviation from $-90°$ ($+90°$) of the actual hybrid. Replacing $\hat{a}^L_{ideal}$ by (A30) in (A12) for T_L gives

$$T'_L = [T_V + e_L T_H + \sqrt{e_L}(T_3 \sin\phi_L + T_4 \cos\phi_L)]/(1 + e_L) \tag{A32}$$

and similarly replacing $\hat{a}^R_{ideal}$ by (A31) in (A13) for T_R gives

$$T'_R = [T_V + e_R T_H - \sqrt{e_R}(T_3 \sin\phi_R + T_4 \cos\phi_R)]/(1 + e_R) \tag{A33}$$

where $T'_{L/R}$ are the actual brightness temperatures which would be detected leaving the quadrature hybrid ports. Note that $e_L = e_R = 1$ and $\phi_L = \phi_R = 0$ gives $T'_{L/R} = (T_V + T_H \pm T_4)/2$.

Incoherent measurement of T_4 by a nonideal antenna and hybrid is determined by using (A32) and (A33) in place of (A12) and (A13) in (A15), giving

$$\begin{aligned} T'_{4_{inc}} \equiv T'_L - T'_R &= T_V\left(\frac{1}{1 + e_L} - \frac{1}{1 + e_R}\right) \\ &+ T_H\left(\frac{e_L}{1 + e_L} - \frac{e_R}{1 + e_R}\right) \\ &+ T_3\left(\frac{\sqrt{e_L}\sin\phi_L}{1 + e_L} + \frac{\sqrt{e_R}\sin\phi_R}{1 + e_R}\right) \\ &+ T_4\left(\frac{\sqrt{e_L}\cos\phi_L}{1 + e_L} + \frac{\sqrt{e_R}\cos\phi_R}{1 + e_R}\right) \end{aligned} \tag{A34}$$

Note that as in (A24), $T'_{4_{inc}}$ is also corrupted by a fraction of T_V and T_H. Note also that the imbalance between LHCP and RHCP eccentricities, and not the level of the eccentricity itself, determines the magnitude of this corruption.

Acknowledgments. The author acknowledges the very thorough proofreading, error checking, and insights provided by Dan Walker of Ball Aerospace and Technologies Corp. The anonymous reviewers also contributed to the clarity, presentation, and interpretation of this material. This work was supported in part by the Applied Research Laboratory at Pennsylvania State University under the direction and sponsorship of the Meteorology and Oceanography (METOC) Systems Program Office at SPAWAR, U.S. Navy.

References

Bespalova, Y. A., V. M. Veselov, and V. Y. Gershenzon, Determining surface wind velocity by measurements of polarization anisotropy of natural and scattered microwave radiation, *Issled. Zemli Kosmosa*, *1*, 87–94, 1982.

Etkin, V. S., M. D. Raev, M. G. Bulatov, Y. A. Militsky, and A. V. Smirnov, Radio-hydrophysical aerospace research of ocean, *Rep. IIp-1749*, Space Res. Inst., Russ. Acad. of Sci., Moscow, 1991.

Gaiser, P. W., P. Chang, K. St. Germain, and M. Keller, Airborne polarimetric radiometer retrievals of the ocean surface wind vector, paper presented at the Fifth Specialist Meeting on Microwave Radiometry and Remote Sensing of the Environment, URSI, Boston, Mass., Nov. 4–6, 1996.

Gasiewski, A. J., and J. R. Piepmeier, Polarimetric scanning radiometer for airborne microwave imaging of ocean thermal emission, paper presented at the Fifth Specialist Meeting on Microwave Radiometry and Remote Sensing of the Environment, URSI, Boston, Mass., Nov. 4–6, 1996.

Goodberlet, M. A., C. T. Swift, and J. C. Wilkerson, Remote sensing of ocean surface winds with the special sensor microwave imager, *J. Geophys. Res.*, *94*(C10), 14,547–14,555, 1989.

Hagen, J. B., and D. T. Farley, Digital-correlation techniques in radio science, *Radio Sci.*, *8*(8–9), 775–784, 1973.

Ishimaru, A., *Electromagnetic Wave Propagation, Radiation, and Scattering*, 637 pp., Prentice-Hall, Englewood Cliffs, N. J., 1991.

Njoku, E. G., E. J. Christensen, and R. E. Cofield, The SeaSat scanning multichannel microwave radiometer (SMMR): Antenna pattern correction development and implementation, *IEEE J. Oceanic Eng.*, *5*(2), 125–137, 1980.

Skou, N., and B. Laursen, Measurement of ocean wind vector by an airborne, imaging, polarimetric radiometer,

paper presented at the Fifth Specialist Meeting on Microwave Radiometry and Remote Sensing of the Environment, URSI, Boston, Mass., Nov. 4–6, 1996.

Sollner, M., and H. Suss, Design and first experimental results of a full-polarimetric quasioptical radiometer system at 90 GHz with high spatial, radiometric and polarimetric resolution, paper presented at the Fifth Specialist Meeting on Microwave Radiometry and Remote Sensing of the Environment, URSI, Boston, Mass., Nov. 4–6, 1996.

Wentz, F. J., Measurement of oceanic wind vector using satellite microwave radiometers, *IEEE Trans. Geosci. Remote Sens*., *30*(5), 960–972, 1992.

Wilheit, T. T., and A. T. C. Chang, An algorithm for retrieval of ocean surface and atmospheric parameters from the observations of the scanning multichannel microwave radiometer, *Radio Sci*., *15*(3), 525–544, 1980.

Wilson, W. J., and S. H. Yueh, Ocean wind direction measurements using passive polarimetric radiometers, *JPL Publ. D96-6*, 44 pp., 1996.

Yueh, S. H., S. V. Nghiem, R. Kwok, W. J. Wilson, F. K. Li, J. T. Johnson, and J. A. Kong, Polarimetric thermal emission from periodic water surfaces, *Radio Sci*., *29*(1), 87–96, 1994a.

Yueh, S. H., R. Kwok, F. K. Li, S. V. Nghiem, W. J. Wilson, and J. A. Kong, Polarimetric passive remote sensing of ocean wind vectors, *Radio Sci*., *29*(4), 799–814, 1994b.

Yueh, S. H., W. J. Wilson, F. K. Li, S. V. Nghiem, and W. B. Ricketts, Polarimetric measurements of sea surface brightness temperatures using an aircraft K-band radiometer, *IEEE Trans. Geosci. Remote Sens*., *33*(1), 86–92, 1995.

C. S. Ruf, Department of Electrical Engineering, Pennsylvania State University, 121 Electrical Engineering East, University Park, PA 16802. (e-mail: ruf@ktb.ee.psu.edu)

(Received July 1, 1997; revised August 21, 1998;
accepted August 25, 1998.)